

1 *Supplement of*  
2 **Aerosol formation and growth rates from chamber experiments**  
3 **using Kalman smoothing**  
4 **Matthew Ozon et al.**

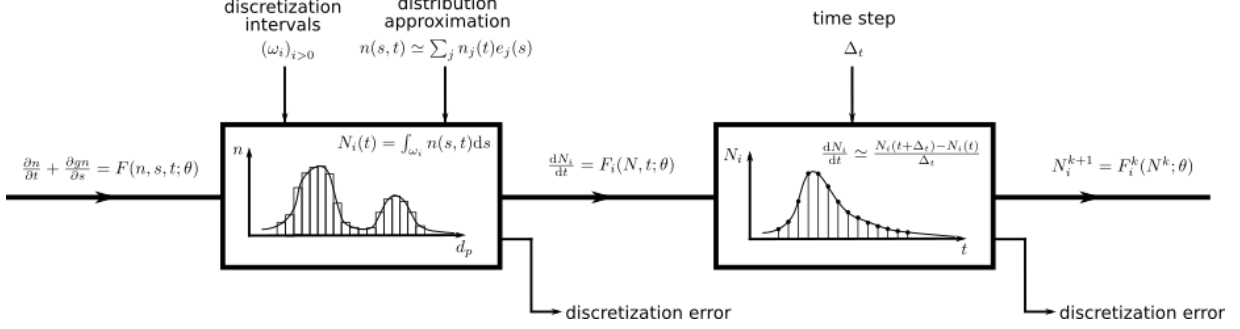
5 **S1 Used assumptions for the Extended Kalman Filter**

	Quantity	simulated data	H <sub>2</sub> SO <sub>4</sub> -NH <sub>3</sub>	$\alpha$ -pinene ozonolysis	HIO <sub>3</sub>	
time step	$\Delta_t$ [s]		40		1.82	
size-	$q$ [-]		16		32	
discretization	$d_0$ [nm]		1.795		1.747	
$d_i = d_0 r^{i-1}$	$r$ [-]		1.117		1.057	
growth rate $g$	$g^{0 0}$ [nm h <sup>-1</sup> ]			$10^{-3}$		
	$\Gamma_g^{0 0}$ [nm <sup>2</sup> h <sup>-2</sup> ]		1		0.25	
	$\sigma_g$ [nm h <sup>-1</sup> ]		1		1.25	
	$T_g$ [s]		300		60	
	$\zeta_g$ [-]			0.95		
	$\delta_g$ [-]	0.4l = 6.4	6.4	6.4	6.4	12.8
	$a_g$ [-]				2	
loss rate $\lambda$	$\lambda^{0 0}$ [s <sup>-1</sup> ]		$\lambda_{wall}^{0 0} = 1.63 \cdot 10^{-3} / d_p[\text{nm}]$			
	$\Gamma_\lambda^{0 0}$ [s <sup>-2</sup> ]		$\lambda_{dil}^{0 0} = 1.72 \cdot 10^{-4}$	$\lambda_{dil}^{0 0} = 1.58 \cdot 10^{-4}$	$\lambda_{dil}^{0 0} = 1.72 \cdot 10^{-4}$	
	$\sigma_\lambda$ [s <sup>-1</sup> ]			$(0.1 \lambda^{0 0})^2$		
	$\delta_\lambda$ [-]		0.1l = 1.6		10 <sup>-7</sup>	
	$a_\lambda$ [-]				1	
nucleation rate $J$	$J^{0 0}$ [cm <sup>-3</sup> s <sup>-1</sup> ]		0.07		1.39	
	$\Gamma_J^{0 0}$ [cm <sup>-6</sup> s <sup>-2</sup> ]		0.25		100	
	$\sigma_J$ [cm <sup>-3</sup> s <sup>-1</sup> ]		0.5		10	
	$T_J$ [s]		300		60	
	$\zeta_J$ [-]			0.95		
size-distribution	$N^{0 0}$ [cm <sup>-3</sup> ]			0		
$N$	$\Gamma_N^{0 0}$ [cm <sup>-6</sup> ]			$(10\Delta_i)^2$		
measurement			$\Delta H = 0.5 \cdot (\alpha H +  H(d + \delta_d) - H(d) )$			
error model	$\alpha$ [-]	0.2		0.5		
	$\delta_d$ [nm]			$2.3 \cdot 10^{-3} d_i$		

6 **Table S1:** Used assumptions for the Extended Kalman Filter for all datasets.

## 7 S2 Source of errors in the discrete aerosol general dynamics equation (GDE)

8 The state equations (Eq. (3) and Eq. (4)) include the noise terms  $w^k$  and  $e^k$ , which are approximated as Gaussian errors.  
 9 These terms include errors due to discretization, model and parameter uncertainties, as the problem is formulated in a  
 10 discretized space with uncertainties on both the evolution and measurement model as well as uncertainties on the  
 11 parameters governing the evolution model. The discretization in size and time is illustrated in Fig. S1. In the following,  
 12 we derive expressions, which approximate these error terms, such that their relative magnitudes can be estimated.



13  
 14 **Figure S1:** Schematic view of the discretization process of the aerosol GDE in the FIKS framework. The discretization is a two-step  
 15 process, 1) the size discretization by integration of the GDE over many size intervals (or bins) produces a collection of time ordinary  
 16 differential equations describing the evolution of the concentrations in each size interval, and 2) the time discretization converting the  
 17 time ordinary differential equations into difference equations (e.g. in the most simple case an Euler scheme, i.e.  $\frac{dN_i}{dt} = \frac{N_i(t+\Delta_t) - N_i(t)}{\Delta_t}$ ).

### 18 S2.1 Size discretization

19 We start with the discretization in size, which could be a potential source of error as illustrated in Fig. 1. We used 16  
 20 discretization intervals from 1-10 nm for all presented results, except for the iodine acid experiment where we used 32  
 21 discretization intervals. The discretization in size affects the kernel functions ( $H^k$ ; Fig. 1) but also the size distribution  
 22 ( $N_i^k$ ), the evolution model ( $F(X^k)$ ), and the process parameters ( $g^k, \lambda^k, J^k$ ).

#### 23 S2.1.1 Size distribution approximation

24 The usual way to discretize the time-size population balance equations for aerosols includes as first step an integration  
 25 over size intervals to get a system of time-ordinary-differential-equations. The discretization is introducing errors whose  
 26 amplitude depends mostly on the coarseness of the discretization grid. An illustrative sketch of this discretization  
 27 procedure is given in Fig. S2. The simplified practical relation between the approximated size-distribution  $\hat{n}$  from the  
 28 discretized concentrations  $(N_i)_{i>0}$  is given by:

$$29 \hat{n}(d, t) \triangleq \sum_{i=1}^M \frac{N_i}{\Delta_i} I_{\omega_i}(d) \quad (S1)$$

30 where the rectangular function  $I_{\omega_i}(d)$  is defined as 1 over the interval  $\omega_i$  and 0 anywhere else. The higher order terms  
 31  $O((d - d_i)^2)$  can be neglected for small size intervals where  $d \sim d_i$ . Therefore, the true size distribution can be locally  
 32 approximated by a linear function shown by the blue solid line in Fig. S1. Now, we formulate the error  $\varepsilon_i^N(d)$  between  
 33 the true and the approximated size distribution for each interval  $\omega_i$ :

$$34 \varepsilon_i^N(d) = n(d) - \hat{n}(d) = n(d_i) + \frac{\partial n}{\partial d}(d_i)(d - d_i) + O((d - d_i)^2) - \frac{N_i}{\Delta_i} \quad (S2)$$

35 where  $O$  represents all terms of higher order and the time variable is dropped for clarity. If the size distribution at the  
 36 centroid diameter  $n(d_i)$  is assumed to be the mean value  $\frac{N_i}{\Delta_i}$ , then Eq. (3) can be simplified. As depicted in Fig. S2 the  
 37 size distribution must take the mean value at least once over the size interval  $\omega_i$  (at  $d = \bar{d}_i$  in Fig. S1). We integrate the

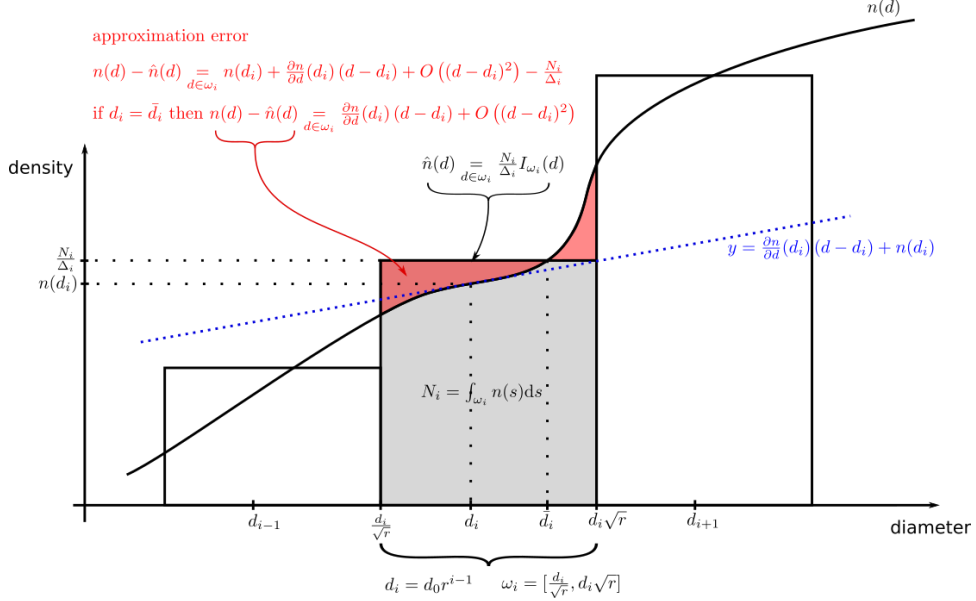
38 error term over the size-interval, which is by definition 0 (as the Taylor Series is an exact approximation if it includes all  
 39 higher order terms), and obtain:

$$40 \quad 0 \stackrel{\text{def}}{=} \int_{\omega_i} \varepsilon_i^N(s) ds = n(d_i) \Delta_i + \frac{\partial n}{\partial d}(d_i) \Delta_i \left( \frac{d_i \sqrt{r} + d_i}{2} - d_i \right) + O(\Delta_i^3) - N_i \quad (\text{S3})$$

41 which allows for the definition of the error  $\varepsilon_i^N$  by expressing the approximation  $n(d_i) \Delta_i$  through the Taylor series:

$$42 \quad \varepsilon_i^N = N_i - n(d_i) \Delta_i = \frac{\partial n}{\partial d}(d_i) \frac{(\sqrt{r}-1)^2}{r-1} \frac{\Delta_i^2}{2} + O(\Delta_i^3) \quad (\text{S4})$$

43 It can be seen that the error approaches 0, if  $r$  approaches 1, which means that the error is getting smaller as the size  
 44 intervals shrinks.



45  
 46 **Figure S2:** Representation of the sources of errors in the discretization of the size-distribution. The black curve is the true size-  
 47 distribution  $n$  and the black rectangles represent the zeroth order approximation  $\hat{n}$ . The red shaded area indicates the absolute error  
 48 over the size interval  $\omega_i$ , while the blue dashed line gives the first order Taylor approximation of  $n$  around the centroid diameter  $d_i$  of  
 49 the  $i^{\text{th}}$  bin.  $\bar{d}_i$  is the diameter for which the true size-distribution  $n$  intersects with its approximation  $\hat{n}$ , which is not necessarily equal  
 50 to the bin's centroid  $d_i$  and is potentially not unique.

### 51 S2.1.2 GDE size-integration using the size distribution approximation

52 The size discretization of the size-distribution will also influence the evaluation of the general dynamics equation (GDE),  
 53 i.e. the evolution model  $F(X^k)$ . Our exemplary derivation of the error term resulting from the discretization of the GDE  
 54 only includes condensation/evaporation growth ( $g$ ) and linear losses ( $\lambda$ ) terms, but neglects the coagulation terms. The  
 55 integral form of the GDE for each size interval  $\omega_i$  is given by:

$$56 \quad \int_{\omega_i} \left( \frac{\partial n}{\partial t}(s, t) + \frac{\partial g n}{\partial s}(s, t) \right) ds = - \int_{\omega_i} \lambda(s, t) n(s, t) ds \quad (\text{S5})$$

57 Again dropping the time variable for clarity and by assuming well-behaved functions for the left-hand side term, namely  
 58 the differentiation under the integral sign, we obtain:

$$59 \quad \frac{dN_i}{dt} + g(d_i^+) n(d_i^+) - g(d_i^-) n(d_i^-) = - \int_{\omega_i} \lambda(s) n(s) ds \quad (\text{S6})$$

60 where  $d_i^+ = d_i \sqrt{r}$  and  $d_i^- = \frac{d_i}{\sqrt{r}}$  are the lower and upper end of the size interval. Using the approximation Eq. (S4):

$$61 \quad \frac{dN_i}{dt} + \frac{g(d_i^+) N_i}{\Delta_i} - \frac{g(d_i^+) \varepsilon_i^N}{\Delta_i} - \frac{g(d_i^-) N_{i-1}}{\Delta_{i-1}} + \frac{g(d_i^-) \varepsilon_{i-1}^N}{\Delta_{i-1}} = - \int_{\omega_i} \lambda(s) n(s) ds \quad (\text{S7})$$

62 The right-hand side is approximated by a first-order expansion and by introducing the mean value of the linear losses in  
63 the size interval  $\bar{\lambda}_i = \frac{1}{\Delta_i} \int_{\omega_i} \lambda(s) ds$ , we obtain:

$$\begin{aligned}
64 \int_{\omega_i} \lambda(s) n(s) ds &= n(d_i) \int_{\omega_i} \lambda(s) ds + \int_{\omega_i} \lambda(s) \left( \frac{\partial n}{\partial s}(d_i)(s - d_i) + O((s - d_i)^2) \right) ds \\
65 &= n(d_i) \int_{\omega_i} \lambda(s) ds + \lambda(d_i) \frac{\partial n}{\partial d}(d_i) \int_{\omega_i} (s - d_i) ds + \int_{\omega_i} O((s - d_i)^2) ds \\
66 &= n(d_i) \int_{\omega_i} \lambda(s) ds + \lambda(d_i) \frac{\partial n}{\partial d}(d_i) \frac{(\sqrt{r}-1)^2}{r-1} \frac{\Delta_i^2}{2} + O(\Delta_i^3) \\
67 &= n(d_i) \bar{\lambda}_i \Delta_i + \lambda(d_i) \frac{\partial n}{\partial d}(d_i) \frac{(\sqrt{r}-1)^2}{r-1} \frac{\Delta_i^2}{2} + O(\Delta_i^3) \tag{S8}
\end{aligned}$$

68 by substituting  $n(d_i)$  through the approximation of Eq. (S4):

$$69 \int_{\omega_i} \lambda(s) n(s) ds = N_i \bar{\lambda}_i + \frac{\partial n}{\partial d}(d_i) \frac{(\sqrt{r}-1)^2}{r-1} \frac{\Delta_i^2}{2} (\lambda(d_i) - \bar{\lambda}_i) + O(\Delta_i^3). \tag{S9}$$

70 Observing that  $\lambda(d_i) - \bar{\lambda}_i = \frac{\partial \lambda}{\partial d}(d_i)(\bar{d}_i - d_i) + O((\bar{d}_i - d_i)^2)$  and that  $\bar{d}_i \in \omega_i$  ( $|\bar{d}_i - d_i| \leq \Delta_i$ ), then:

$$71 \int_{\omega_i} \lambda(s) n(s) ds = N_i \lambda(d_i) - N_i \frac{\partial \lambda}{\partial d}(d_i)(\bar{d}_i - d_i) + O(\Delta_i^2) \tag{S10}$$

72 Now, putting back together all the terms:

$$73 \frac{dN_i}{dt} + \frac{g(d_i^+) N_i}{\Delta_i} - \frac{g(d_i^-) N_{i-1}}{\Delta_{i-1}} = -N_i \lambda(d_i) + W_i^{\text{GDE}} \tag{S11}$$

74 with

$$75 W_i^{\text{GDE}} = N_i \frac{\partial \lambda}{\partial d}(d_i)(\bar{d}_i - d_i) + \frac{g(d_i^+) \varepsilon_i^N}{\Delta_i} - \frac{g(d_i^-) \varepsilon_{i-1}^N}{\Delta_{i-1}} + O(\Delta_i^2) \tag{S12}$$

76 The discretization error of the size-distribution evolution model (i.e. the GDE;  $W_i^{\text{GDE}}$ ) can be written using the explicit  
77 form of  $\varepsilon_i^N, N_i$  (Eq. (S4)) and summarizing all terms of order  $\Delta_i^2$  leads to:

$$78 W_i^{\text{GDE}} = \left( g(d_i^+) \frac{\partial n}{\partial d}(d_i) - \frac{1}{r} g(d_i^-) \frac{\partial n}{\partial d}(d_{i-1}) \right) \frac{(\sqrt{r}-1)^2}{2(r-1)} \Delta_i + O(\Delta_i^2) \tag{S13}$$

79 From Eq. (S13) we see that the discretization error is of first order error whose linear coefficient depends on the size  
80 distribution, its first derivative and the growth rate. Note, that the linear loss terms are of second order in  $\Delta_i$  and hence  
81 not considered further. If the order of magnitude of the error needs to be estimated, these values need to be roughly  
82 estimated. Altogether, it is obvious that if  $r \rightarrow 1$ ,  $\Delta_i \rightarrow 0$  and the error collapses.

## 83 S2.2 Time discretization and estimate of $\Gamma_N^k$

84 The time discretization of the GDE corresponds to the second panel of the block diagram in Fig. S1. The GDE is described  
85 as a system of ordinary differential equations:

$$86 \frac{dN_i}{dt} + \frac{g(d_i^+)}{\Delta_i} N_i - \frac{g(d_i^-)}{\Delta_{i-1}} N_{i-1} = -N_i \lambda(d_i) + W_i$$

87 This set of equations is discretized into difference equations for the time series  $(t_k)_{k \geq 0}, t_k = t_{k-1} + \delta^k$ . We use the  
88 notations  $N_i^k = N_i(t_k), g_i^k = g(d_i^+, t_k), \lambda_i^k = \lambda(d_i, t_k), W_i^k = W_i(t_k)$  for all  $i$  and  $k$ , with  $g_0^k = g(d_1^-, t_k)$ . Using an  
89 explicit Euler scheme, we obtain the size-and-time discretized GDE:

$$90 N_i^{k+1} = N_i^k + \delta^k \left( \frac{g_{i-1}^k}{\Delta_{i-1}} N_{i-1}^k - \frac{g_i^k}{\Delta_i} N_i^k - \lambda_i^k N_i^k \right) + (w_N^k)_i \tag{S14}$$

91 with  $(w_N^k)_i = \delta^k W_i^k + O((\delta^k)^2)$  the total error of the GDE part of the evolution model in Eq. (3), which is used as the  
92 estimate for  $\Gamma_N^k$  in the prediction step of the Extended Kalman Filter (Table 1, Algorithm 1).

93 Overall, we can conclude that the error due to the discretization of the GDE (time and size) is proportional to both, the  
 94 size step and the time step, with a proportionality coefficient depending on the first derivative of the size distribution and  
 95 the growth rate. From this set of difference equations, we can also easily infer a stability (non-divergent) and non-  
 96 oscillatory criteria for fine size-and-time discretization (Gottlieb and Shu, 1998):

$$97 \quad \forall i, k, \delta^k \left( \frac{g_i^k}{\Delta_i} + \lambda_i^k \right) \leq \frac{1}{2}. \quad (\text{S15})$$

98 Hence, the discretized GDE in Eq. (S14) can only lead to physically meaningful solutions if the overall growth is slow  
 99 enough for the chosen discretization grid. Consequently, if numerical diffusion is minimized by choosing a fine size  
 100 discretization grid, also a proper time discretization grid satisfying the criteria in Eq. (S15) needs to be chosen. However,  
 101 for a fine enough time discretization there might be not enough available measurements  $l$ . We therefore use a zero-padding  
 102 technique to emulate a better time resolution, although the measurement operator has to change in time accordingly. The  
 103 operator  $H^k$  should be set to the null operator (a matrix full of zeros) for the instants when the data have been set to zero.  
 104 This way, the measurement update is non-informative and the estimates only rely on the model. In other words, the  
 105 evolution model is computed several times for each actual instant of the dataset.

### 106 S2.3 Measurement operator discretization

107 Last, also the observation model includes an error term  $v^k$ , which apart from the measurement noise (first dropped here  
 108 for simplicity), includes errors of the measurement operator. In the continuous case, the measured counts for channel  $i$   
 109 are given by the equation:

$$110 \quad C_i^* = \int_0^\infty H_i^*(s; \theta) n(s) ds \quad (\text{S16})$$

111 for the continuous size distribution  $n$  and channel efficiency  $H_i^*$  with parameters  $\theta$ . However, the modeled counts  $C_i$   
 112 suffer from errors in the measurement model, which originate from either a discretization error  $\varepsilon_i^H$  or wrong assumptions  
 113 in the measurement model  $e_i^H$ . Formally, the discrepancy between the true and the modeled counts can be written as:

$$114 \quad C_i^* - C_i = \varepsilon_i^H + e_i^H = \int_0^\infty H_i^*(s; \theta) n(s) - H_i(s; \theta) \hat{n}(s) ds \quad (\text{S17})$$

115 Using Eq. (S1) and  $H_i^* = H_i + \Delta H_i$ , we obtain for the discretization error:

$$116 \quad \varepsilon_i^H = \sum_{j=1}^M \int_{\omega_j} \left( \frac{\partial n}{\partial s}(d_j)(s - d_j) + O((s - d_j)^2) \right) H_i^*(s; \theta) ds \quad (\text{S18})$$

117 This can further be expanded, using the Taylor expansion,  $H_i^*(s; \theta) = H_{i,j}^* + O(d - \bar{d}_j)$  around  $\bar{d}_j$ , which is the value  
 118 of the diameter for which  $H_i^*(\bar{d}_j; \theta) = H_{i,j}^*$ :

$$119 \quad \varepsilon_i^H = \sum_{j=1}^M \frac{\partial n}{\partial d}(d_j) \frac{(\sqrt{r}-1)^2 \Delta_j^2}{r-1} H_{i,j}^* + O(\Delta_j^3) \quad (\text{S19})$$

120 Similarly, the modeling error can be expressed as:

$$121 \quad e_i^H = \sum_{j=1}^M n(d_j) \int_{\omega_j} \Delta H_i(s; \theta) ds \quad (\text{S20})$$

122 Rearranging the terms to form the total error  $v_i = \varepsilon_i^H + e_i^H + \Delta y_i$  (including now the measurement noise  $\Delta y_i$ ), and  
 123 using the notation  $\Delta \Psi_{i,j}$  for the averaged value of the operator modeling error, one gets:

$$124 \quad v_i = \Delta y_i + \sum_{j=1}^M n(d_j) \Delta H_{i,j} \Delta_j + \frac{\partial n}{\partial d}(d_j) \frac{(\sqrt{r}-1)^2 \Delta_j^2}{r-1} H_{i,j}^* + O(\Delta_j^3) \quad (\text{S21})$$

125 It can be seen that the numerical value  $v_i$  is either of order 1 or 2 in  $\Delta_j$ . If the measurement model is perfectly known, the  
 126 error is of order 2, but if the measurement model is uncertain, then the error becomes a first order — making the  
 127 discretization error negligible and hence justifying the choice of neglecting the measurement operator discretization error

128 in the used analysis. This estimate of  $v_i$  is then used to compute the covariance  $\Gamma_v^k$  in the Kalman gain matrix (see Eq.  
129 (10) and Eq. (11)) of the Extended Kalman Filter (Table 1, Algorithm 1).